Proceedings of IMECE05
2005 ASME International Mechanical Engineering Congress
November 5-11, 2005, Orlando, FL USA

IMECE2005-82826

INVESTIGATION OF THE EFFECTS OF SLIDING ON WHEEL TREAD DAMAGE

Brandon Talamini
Jeff Gordon
U.S. Department of Transportation
John A. Volpe National Transportation Systems Center
Cambridge, MA 02142 USA

A. Benjamin Perlman
Department of Mechanical Engineering
Tufts University
Medford, MA 02155 USA

ABSTRACT

Wheel tread spalling is the main source of damage to wheel treads and a primary cause for wheel removals from service. Severe frictional heating of the wheel-rail contact patch during sliding causes the formation of martensite, a hard, brittle microstructure. The martensite patches break away from the more resilient bulk of the wheel tread when subjected to contact loads, resulting in spall formation. Prolonged sliding allows a greater volume of wheel tread material to reach extremely high temperatures, which will lead to material ablation and the formation of a slid flat. Such flats are the cause of wheel impact loads, which are extremely damaging to truck components and rail. This paper outlines an approach developed to estimate the effects of sliding on wheel flat formation and the potential severity of spalling. The methodology is described and preliminary results are presented using an intentionally simplified idealization of the wheel-rail contact geometry. Material characterization (temperature-dependent properties and failure criteria) and management of model size are of equal importance to geometric fidelity and are the focus in the early stages of the development of the qualitative model present here.

INTRODUCTION

Wheel sliding, caused by railcar movement with stuck brakes or engaged handbrakes, creates two significant problems for the industry. Severe heating of the wheel tread material during sliding causes thermal damage that can lead to spalling. Prolonged sliding promotes the formation of slid flats that, in turn, create large impact loads that damage the rail, bearings, and other equipment. Spalling and slid flats ultimately lead to increased maintenance costs and equipment downtime. This work seeks to develop an understanding of the two processes. Knowledge of the temperature gradients generated in a sliding wheel can be used to refine ongoing efforts to develop wheel alloys that may prove more resistant to spalling. Estimates of the load magnitude and slide distance required to cause the formation of slid flats of a given length can be used to estimate the effect of impact load stresses on the fatigue performance of freight wheels.

Flat formation is simulated by removing wheel material when prescribed failure criteria are exceeded. The extent of spalling is estimated by the depth of penetration into the tread of wheel material that has undergone a transformation to martensite due to the temperature gradient resulting from the frictional heat generated during sliding. The approach can be used investigate the rate of wheel flat formation with different wheel and rail geometry, load magnitude, slide speed, distance, material properties, and heat treatment.

A qualitative model was constructed with simplified geometry as a proof-of-concept and to establish a method of addressing wheel sliding and ablations problems. This construction of this model is the subject of the current paper. The model can be extended with exact wheel and rail geometry and particular braking patterns as necessary, and in fact, the authors are continuing research in this direction following the completion of this paper.

The method of addressing wheel ablation is illustrated below with the simple qualitative model. First, an idealized model was conceived to pose the problem in a suitable form. This concept is described first. The implementation of this concept in the finite element method is then illustrated.

IDEALIZED MODEL

The conceptual model consists solely of a wheel and a rail (see Figure 1). The wheel slides along the rail at constant velocity, with friction generating heat the wheel-rail interface. The load on the wheel is the wheel's nominal share of a standard railcar's dead weight, 147 kN (33000 lb). This load does not vary, and the wheel remains in equilibrium. The frictional heating and sliding lead to ablation of the wheel material in the neighborhood of the contact interface.

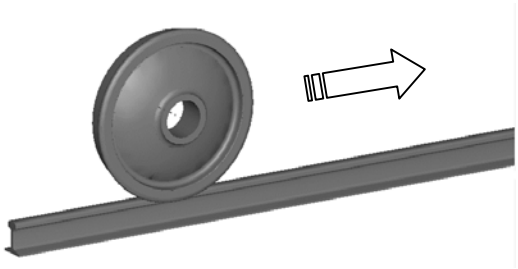

Figure 1 Idealized model.

IMPLEMENTATION

The finite element model is designed to capture the key features of the idealized model. Some of the features require approximation in the finite element scheme. The geometry of the rail and wheel are greatly simplified for this paper (see Figure 2). The simplified geometry reduces the computational effort significantly, and allows the research to be concentrated on the modeling process. The geometry will be elaborated upon in future research.

The wheel is generalized as a disc. Only half of the disc is modeled since the regions of the wheel remote from the contact surface do not have much influence on the heating and wearing phenomena. The radius of the wheel is 457 mm, and it is 8 cm thick. The rail is simply a rectangular prism 20 cm high. The thickness is exactly the same as the wheel, and contains the same number of elements as the wheel model through the thickness so that the aspect ratios of the contacting elements are the same. This improves the accuracy of the contact stresses given the intentionally crude mesh. It should be noted that a model with more geometric fidelity would require many more elements in the vicinity of the contact interface to obtain accurate stresses and wear patterns.

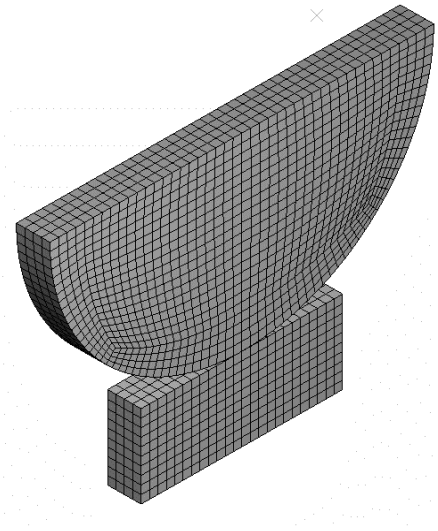

Figure 2 Finite element model.

The rail mesh is created using the arbitrary Lagrangian-Eulerian (ALE) surface feature in ABAQUS [1]. This feature is utilized so that the model of the rail does not need to extend the entire length of the wheel sliding distance. Instead, the mesh is similar to a control volume: The cross-sectional surfaces at the ends of the rail are Eulerian, allowing material to enter and exit. The other mesh surfaces are "sliding" surfaces [1], which deform with the underlying material in the direction of the surface normal to capture the contact deformation, but allow material to freely flow past nodal points in directions parallel to the surfaces (see Figure 3). The interior nodes of the rail mesh all use Eulerian reference frames and hence do not follow the material flow. The wheel is modeled with a standard Lagrangian mesh and does not move in a rigid body sense. The wheel remains stationary as the rail material slides underneath it. The simulation may be carried out for as long as is desired without requiring remeshing.

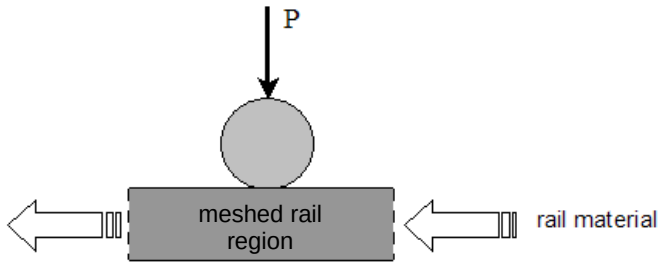

Figure 3 Model schematic.

The idealized model is essentially quasi-static; however, the explicit time-integration solver ABAQUS/Explicit is employed to take advantage of the material failure and removal models available. The material modeling is described in detail later.

Hexahedral coupled temperature-displacement elements with trilinear interpolation are used exclusively (C3D8T elements in the ABAQUS library). The wheel is composed of 3744 elements and 4975 nodes; the rail is composed of 1360 elements and 1925 nodes. The elements are roughly cubical with 2 cm sides.

PROCEDURE

An initial velocity of 2.24 m/s (5 mph) is prescribed for the rail material and is maintained throughout the analysis with inflow and outflow velocity boundary conditions (see Figure 4). Coulomb friction is defined between the wheel and the rail material with a coefficient of 0.2. No temperature dependence is defined for this quantity.

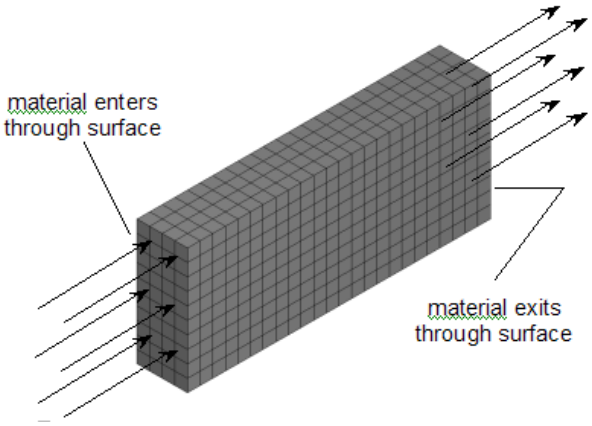

Figure 4 Rail mesh showing Eulerian surfaces.

The nominal wheel load is distributed over the exposed wheel cross-section (only half of the wheel is modeled – see Figure 2). The temperature and mechanical response of the wheel and rail are calculated simultaneously in an explicit time integration scheme.

Slip between the wheel nodes and the moving rail material creates frictional heating at the interface. During the analysis elements fail according to the damage model and are automatically deleted. Thermal properties for the wheel and rail materials are given in the Appendix.

Mechanically, the rail mesh is constrained to prevent rigid body motion. The temperature of the new rail as it enters the control volume is prescribed at an assumed ambient temperature of 20˚C (68 ˚F). Nodes in the exposed cross-section of the wheel are constrained to move only in the vertical direction. This prevents the wheel from rolling or moving off of the rail. The vertical position of the wheel is maintained by contact with the rail.

MATERIAL MODEL

The material properties of the wheel material are assumed to be those of an Association of American Railroads class B wheel [2] (see Table 1).

Table 1 Material properties of AAR class B wheel steel.

Yield strength	550 MPa (80 ksi)
Ultimate strength	900 MPa (130 ksi)
Elongation at break	8%

The elastic response of the wheel and rail materials is modeled with temperature dependent linear elasticity. The Young's modulus and Poisson's ratio are specified as tabulated data by temperature value and are typical for steel; the values used are located in the Appendix. The density is assumed to have a constant value of 7861 kg/m^3. Identical elastic properties are used for the rail and wheel materials.

The Johnson-Cook kinematic hardening model is used for plasticity calculations for the wheel material because its use allows access to the shear failure material model in ABAQUS. The von Mises theory is used to predict yielding. The yield strength evolves according to the equation[1] [3]

$$\sigma_0 = \left[A + B(\bar{\varepsilon}_{pl})^n\right]\left(1 - \theta^m\right), \qquad (1)$$

where A is the yield strength of the virgin material at a reference temperature, B and n are material constants determined through testing, $\bar{\varepsilon}_{pl}$ is the equivalent plastic strain, and θ is a dimensionless temperature defined as

$$\theta = \begin{cases} 0 & T < T_{tr} \\ \dfrac{T - T_{tr}}{T_m - T_{tr}} & T_{tr} \le T \le T_m \\ 1 & T > T_m \end{cases}. \qquad (2)$$

In Eq. 2, T_{tr} and T_m are the "transition" temperature and the "melting" temperature, respectively. The transition temperature is defined as the lowest temperature at which yield strength temperature dependence is observed. The melting temperature is defined such that the material loses all shear resistance at or above it. Put another way, the transition and melting temperature define the range where the material exhibits yield strength temperature dependence.

Typically, a bilinear material model is used to characterize the behavior of wheel steels in numerical analyses at plastic strains that are small with respect to the ultimate strain [4]. The hardening slope is usually approximated as one-tenth of the elastic modulus. However, this response is too stiff at large plastic strains. For the present analysis, the Johnson-Cook material constant B and the strain hardening exponent n are chosen to approximate the bilinear material response at small plastic strains while agreeing with the actual ultimate strain (defined by the percent elongation) at the ultimate strength of the material (see Figure 5). The Johnson-Cook parameters are given in Table 2.

Table 2 Johnson-Cook material parameters for the wheel material.

A	550 MPa (80 ksi)
B	1278 MPa (185 ksi)
n	0.5
m	1

[1] The standard Johnson-Cook model has terms that characterize strain rate effects on the yield stress. These terms are omitted since the wheel loading is nearly quasi-static in this case.

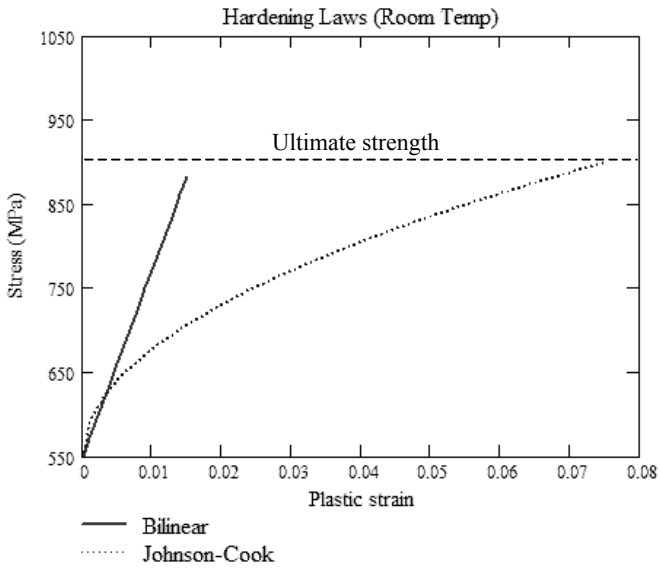

Figure 5 Comparison of a bilinear hardening law with the Johnson-Cook model

Linear temperature dependence of the yield stress is assumed for this model, meaning the value of *m* is taken as 1. The transition temperature is taken as 230°F, and the melting temperature is taken as 700°F. These values are not actual physical constants but are chosen for convenience to approximate the observed behavior of wheel steel seen in reference [2]. A more exact fit can be obtained with a nonlinear relation, but this would unnecessarily complicate the current investigation. The linear model displays reasonable agreement with the observed behavior (see Figure 6).

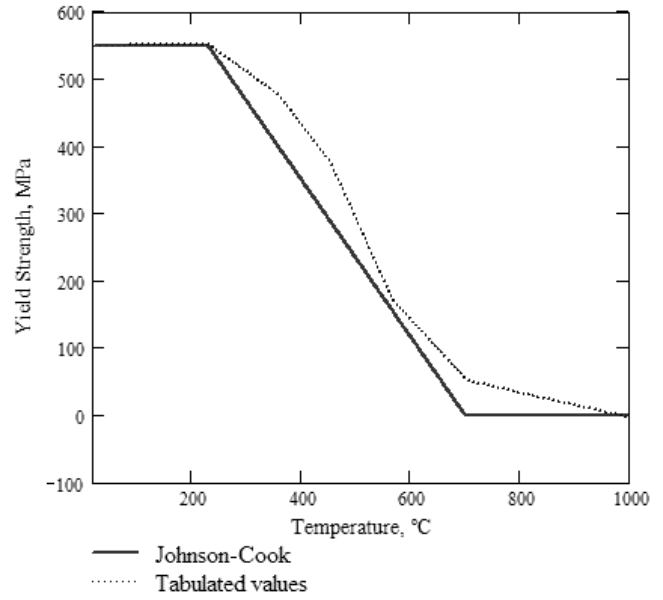

Figure 6 Comparison of yield strength temperature dependence models.

The material removal criterion is a simple equivalent plastic strain cutoff. The cutoff value is taken as the true plastic strain reached at the uniaxial test ultimate strength, which is approximated as the percent elongation at break minus the elastic strain (0.075). Every 10 time increments, the finite element program checks the equivalent plastic strains at all element integration points in the wheel elements. An element is deleted from the analysis when the equivalent plastic strain is found to exceed the cutoff value at all of its integration points.

Plasticity in the rail material is modeled with linear kinematic hardening. The hardening modulus and yield strength are tabulated as functions of temperature. The values are given in the Appendix. The Johnson-Cook hardening model is unnecessary since ablation of the rail does not need to be modeled.

The thermal conductivities, thermal expansion coefficients, and specific heats of the two materials are assumed identical and are tabulated as functions of temperature in the Appendix.

RESULTS

Figure 7 illustrates how the method described above represents the wearing of a wheel. The coarse mesh in Figure 2 was used to demonstrate the methodology. Elements in high stress/high temperature areas of the wheel are ablated; these elements have been removed in the irregular pattern at the bottom of the figure.

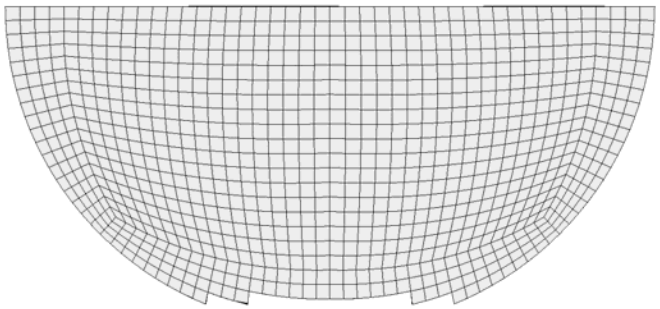

Figure 7 A wheel model after some material has eroded.

The wear pattern is sensitive to the mesh design. A mesh consistent with observed wheel flat geometry is needed to improve the fidelity of the model. With a finer mesh, the worn region takes on a more refined shape. In the top portion of Figure 8 identifies the wear region of the wheel. The result shown in the bottom right portion depicts the coarse mesh at an earlier time then Figure 7. The rough ablation shape is due to the large element size. The result in the left portion shows smoother wear. The elements in this model are one-fourth the size of model in the coarse mesh.

In its current state, the approach can be used to make qualitative comparisons between different materials and different arrangements of car weight, slide time, and slide speed.

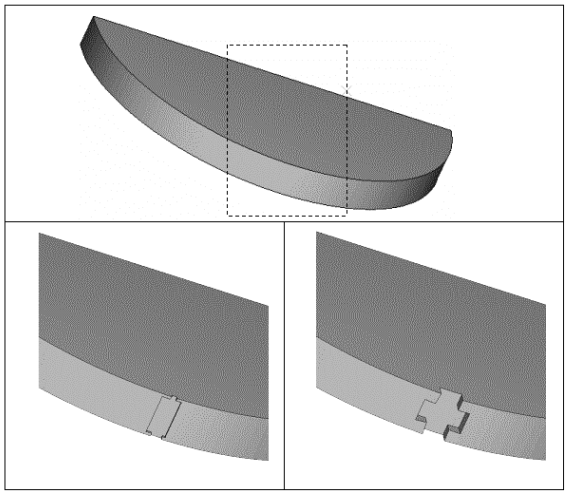

Figure 8 Top: Area of detail. Left: An intermediate state with a fine mesh. Right: An intermediate state with the coarse mesh shown in earlier figures.

A simulation of 10 seconds of real time took approximately 22 hours with a 3 GHz Pentium 4 processor for the coarse mesh. The fine mesh took approximately a week to simulate a 1.5 s slide. The method is computationally intensive due to the small element size required. A geometrically accurate wheel model flat will require a carefully planned mesh and a reliable material representation.

FUTURE RESEARCH

Different slide speeds and two slide distances will be examined in the coming months so that some qualitative comparisons on heating and ablation rates can be made. The depth of the martensitic microstructure change will be estimated by examining the nodal temperature histories of the wheel.

Future investigation in this subject will incorporate a number of improvements. Actual wheel and rail shapes will replace the abstract geometry of the present model. The residual stresses in the wheels following manufacture will be included, following the process established by Gordon and Perlman [4] and Gordon and Orringer [5]. The failure strain in the wheel material model will utilize a function of temperature and stress tri-axiality.

Results of the analyses will be presented for a range of applied vertical wheel loads, sliding distances, and slide speeds.

ACKNOWLEDGMENTS

The work reported in this paper was carried out under the Rail Equipment Safety program sponsored by the Office of Research and Development, Federal Railroad Administration, under the direction of Ms. Claire L. Orth, Chief, Equipment and Operating Practices Research Division. Ms. Monique Stewart is the Project Manager for the work related to railroad wheels.

REFERENCES

[1] ABAQUS/Standard User's Manual (version 6.4-1). ABAQUS, Inc., Warwick, RI, 2003.

[2] Kuhlman, C., Sehitoglu, H., and Gallagher, M., "The Significance of Material Properties on Stresses developed during quenching of Railroad Wheels," Proc. Joint ASME/IEEE Railroad Conference, April, 1998, pp. 55-63

[3] Johnson, G.R., and Cook, W.H., "A Constitutive Model and Data for Metals Subjected to Large Strains, High Strain Rates, and High Temperatures", Proc. Seventh International Symposium on Ballistics, The Hague, The Netherlands, pp. 541-548, April, 1983.

[4] Gordon, J.E. Perlman, A.B. "Estimation of Residual Stresses in Railroad Commuter Car Wheels Following Manufacture." Volpe National Systems Center Report to the Federal Railroad Administration. Report no. DOT/FRA/ORD-03/24. June, 2003

[5] Gordon, J.E. and Orringer, O. "Investigation of the effects of Braking System Configurations on Thermal Input to Commuter Car Wheels." Volpe National Transportation Systems Center Report to the Federal Railroad Administration. Report no. DOT/FRA/ORD-96/01. 1996.

APPENDIX

Wheel Material Properties

Table 3 Coefficient of thermal expansion

Temperature (°C)	α $\times 10^{-6}$
0	9.89
230	10.82
358	11.15
452	11.27
567	11.31
704	11.28
900	11.25

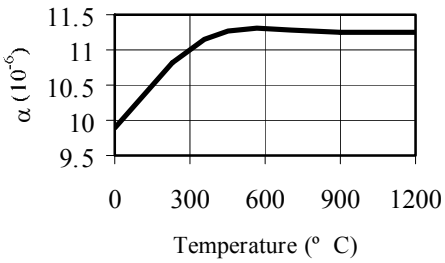

Figure 9 Coefficient of thermal expansion vs. temperature

Table 4 Thermal conductivity

Temperature (°C)	k (W/m-°C)
0	59.71
350	40.88
703	30.21
710	30.00
800	25.00
950	27.05
1200	30.46

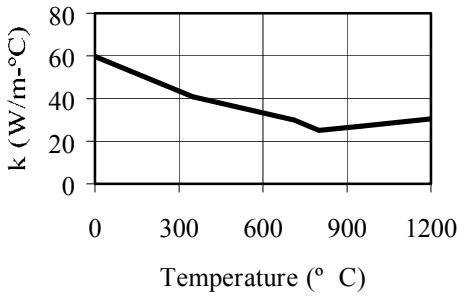

Figure 10 Thermal conductivity vs. temperature

Table 5 Specific heat

Temperature (°C)	c_p (J/kg-°C)
0	419.5
350	629.5
703	744.5
710	652.9
800	657.7
950	665.2
1200	677.3

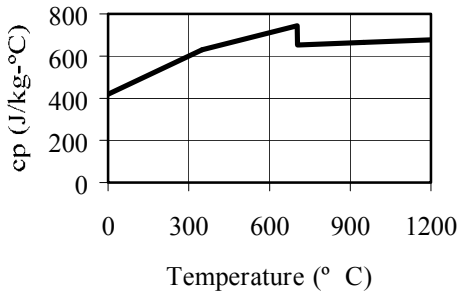

Figure 11 Specific heat vs. temperature

Table 6 Elastic modulus

Temperature (°C)	E (Gpa)
24	213
230	201
358	193
452	172
567	102
704	50
900	43

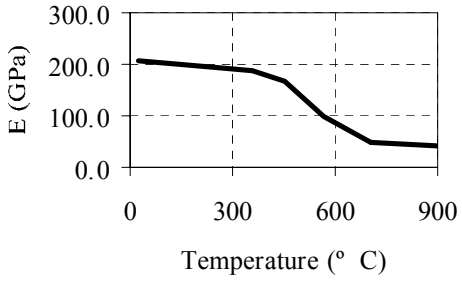

Figure 12 Elastic modulus vs. temperature

Table 7 Poisson's ratio

Temperature (°C)	ν (Gpa)
24	0.295
230	0.307
358	0.314
452	0.32
567	0.326
704	0.334
900	0.345

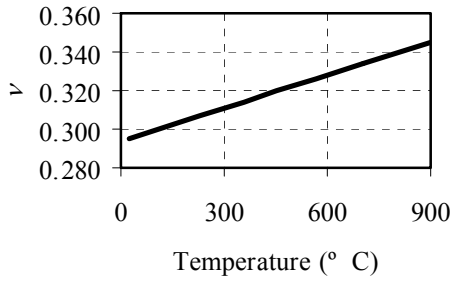

Figure 13 Poisson's ratio vs. temperature

Additional Rail Material Properties

Table 8 Hardening modulus

Temperature (°C)	E_p (MPa)
24	22.7
230	26.9
358	21.3
452	15.6
567	6.2
704	1.0
900	0.1

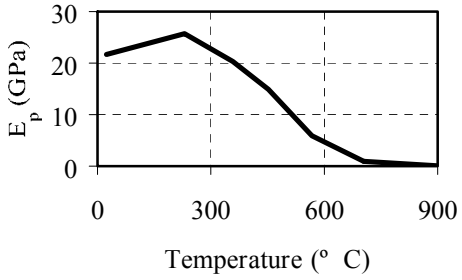

Figure 14 Hardening modulus vs. temperature

Table 9 Yield strength

Temperature (°C)	S_y (MPa)
24	483.0
230	485.1
358	418.8
452	332.4
567	151.1
704	45.0
900	13.4

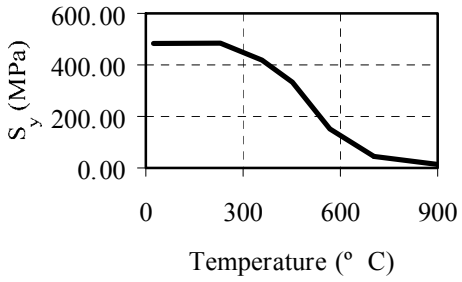

Figure 15 Yield Strength vs. temperature